

18 **ABSTRACT**

19 The global radiative effect of brown carbon (BrC) remains highly uncertain. BrC's
20 photobleaching, which significantly ~~alerts~~ affects its radiative effect, has been still poorly
21 constrained. This study investigates and compares photobleaching rates of laboratory-synthesized
22 secondary BrC (aq-BrC), biomass burning-derived BrC (b-BrC), and ambient PM_{2.5}-derived BrC
23 (p-BrC) to illustrate the variability in BrC photobleaching kinetics from different types of BrC
24 reported in prior studies. Our results reveal a source dependence in BrC photobleaching rates. The
25 highest photobleaching rate constant (k_{BrC}) is observed for aq-BrC ($1.13 \pm 0.08 \text{ h}^{-1}$), followed by
26 p-BrC ($0.12 \pm 0.02 \text{ h}^{-1}$) and b-BrC ($0.05 \pm 0.01 \text{ h}^{-1}$), indicating the stable light-absorption capacity
27 of b-BrC in the atmosphere. Integration of these rate constants with data derived from previous
28 studies highlighted the differences in photobleaching behaviors among BrC from different sources.
29 The OH oxidation of imidazole-2-carboxaldehyde (2-IC) and methylglyoxal oligomers,
30 nitrophenols (including phenols), and lignin derivatives governs the photobleaching of aq-BrC, p-
31 BrC, and b-BrC, respectively. The high k_{BrC} of aq-BrC is attributed to the high reactivity of the
32 chain structures in 2-IC and methylglyoxal oligomers. In contrast, the highly conjugated structures
33 of lignin derivatives in b-BrC impart stability against OH oxidation, resulting in a low k_{BrC} . Our
34 findings reveal the significant differences in the photobleaching behavior of BrC originated from
35 different sources, underscoring the crucial need to account for source differences in assessments
36 of BrC's global radiative forcing effect.

37

38 1. Introduction

39 Brown carbon (BrC) is a significant contributor to atmospheric warming (Saleh, 2020; Chung et al., 2012;
40 Brown et al., 2021) and Earth's radiative budget (Bond, 2001; Kirchstetter et al., 2004; Wang et al., 2018; Wang
41 et al., 2022) due to its ultraviolet-visible (UV-Vis) light absorption. The BrC's direct radiative effect (DRE),
42 accounting for 20%–40% of total DRE caused by light-absorbing carbonaceous aerosols (Heald et al., 2014; Jo
43 et al., 2016; Saleh et al., 2015; Wang et al., 2018; Wang et al., 2014), remains highly uncertainty. BrC with global
44 average DRE values varying from +0.03 to +0.57 W/m² is considered as the least understood warming agents in
45 the atmosphere (Zhang et al., 2020; Zeng et al., 2020; Corr et al., 2012).

46 BrC comprises abundant chemically reactive species that react readily with atmospheric reactive gases and
47 radicals (Aiona et al., 2017; Fleming et al., 2020; Hems et al., 2021; Liu et al., 2020), modifying its light-
48 absorption properties. Both laboratory experiments (Borduas-Dedekind et al., 2019; Fleming et al., 2019; Hems
49 and Abbatt, 2018; Hems et al., 2020; Schnitzler and Abbatt, 2018; Schnitzler et al., 2022) and field campaigns
50 (Dasari et al., 2019; Qiu et al., 2024; Wang et al., 2014; Xu et al., 2024; Zeng et al., 2020) consistently found
51 that BrC's photochemical aging process reduced its mass absorption coefficient (MAC), which is also known as
52 photobleaching. In current models, the evaluation of BrC photobleaching on its radiative forcing [effect](#) mainly
53 depends on the temporal [evolution-decline of in](#) BrC's light-absorption capacity (Schnitzler et al., 2022; Wang
54 et al., 2018; Xu et al., 2024), i.e., the photobleaching rate, which is substantial variability across different
55 laboratory experiments and field observations. Notably, BrC generated from aqueous-phase reactions often
56 exhibits negligible absorbance in the UV-Vis range after less than 2 hours of radiation (Aiona et al., 2017). Field
57 observations reveal that atmospheric BrC undergoes a MAC reduction exceeding 60% after 1 day of sunlight
58 exposure (Müller et al., 2023; Qiu et al., 2024). In comparison, over the same 1 day of solar radiation, the
59 reduction in the MAC of BrC derived from biomass burning is much lower than atmospheric BrC (Fan et al.,
60 2019; Fleming et al., 2020; Müller et al., 2023; Wong et al., 2019). Accurately determining BrC's photobleaching
61 rate is paramount for quantifying the impact of BrC photobleaching on its radiative forcing effect in models.

62 Furthermore, BrC's chemical composition fundamentally governs its photochemical reactivity (Hems et al.,
63 2021; Hems and Abbatt, 2018; Dalton and Nizkorodov, 2021; Liu et al., 2025), thereby modulating its
64 photobleaching rate. However, the relationship between changes in BrC's molecular composition and light
65 absorption properties during the photobleaching is still poorly constrained. This knowledge gap leads to
66 significant uncertainty in evaluating the evolution of BrC's light absorption capacity during atmospheric
67 transportation. For instance, BrC emitted from biomass burning has been observed to retain strong absorption
68 after several days of transport to the Arctic (Yue et al., 2022). In contrast, model simulations estimate BrC is
69 nearly complete photobleaching over this timescale (Wang et al., 2018; Xu et al., 2024), which contradicts the
70 observational evidence. Elucidating the linkage between BrC molecular composition and photobleaching rates
71 would improve the accuracy of global-scale assessments of BrC's dynamic light absorption properties during
72 long-range transport.

73 In this work, we performed photochemical aging experiments on three types of BrC [under identical,](#)
74 [controlled conditions](#), including synthesized by aqueous phase reaction (referred to “aq-BrC”), and extracted

75 from ambient (referred to “p-BrC”, where “p” denotes particulate) and biomass burning (referred to “b-BrC”)
76 PM_{2.5} samples. ~~We found that the photobleaching rates of BrC from different sources vary~~
77 ~~significantly.~~ Compared to previous studies, this work systematically investigated the differences in
78 ~~photobleaching kinetics among various types of BrC under identical environmental conditions.~~ We combine this
79 ~~with high-resolution mass spectrometry (HRMS) analysis to establish a mechanistic link between the observed~~
80 ~~divergent BrC photobleaching rates and the evolution of key molecular chromophores.~~ ~~High-resolution mass~~
81 ~~spectrometry (HRMS) analysis was adopted to provide molecular-level understanding of this source-dependent~~
82 ~~BrC photobleaching rate.~~ In addition, we quantify the contribution of the OH oxidation pathway across all BrC
83 ~~types.~~ OH oxidation was determined as the dominate pathway of BrC photobleaching. These findings aim to
84 ~~provide essential parameters and a mechanistic basis for improving the representation of BrC photochemical~~
85 ~~aging in climate models.~~ ~~highlight the importance of considering differences in BrC sources when assessing its~~
86 ~~global radiative forcing effect.~~

87 2. Methodology

88 2.1 Preparation of BrC

89 Methylglyoxal (MG, 40 wt%, Merck) and ammonium sulfate (AS, 98%, Aladdin) solutions (1 mol/L) was
90 mixed in darkness at room temperature for 2 h (pH 3.7–4.2) (Yang et al., 2024) to generate aq-BrC. Residual
91 MG/AS were removed by solid-phase extraction (SPE) (Lin et al., 2010; Wang et al., 2017). The eluent was
92 dried under gentle stream of ultrapure N₂ (>99.99%) and reconstituted in ultrapure water (18.2 MΩ·cm).
93 ~~Previous studies have confirmed that MG is one of the most abundant dicarbonyl species in the atmosphere (Gu~~
94 ~~et al., 2025; Fu et al., 2008), which is produced by primary emissions and oxidation of volatile organic~~
95 ~~compounds (VOCs). Considering that MG exhibit a tendency to partition into aqueous aerosols and cloud~~
96 ~~droplets in the atmosphere (Laskin et al., 2015), therefore, the secondary BrC generated by the aqueous-phase~~
97 ~~reaction between MG and AS is representative as aq-BrC.~~

98 PM_{2.5} samples emitted from corn straw combustion in household stoves was collected on quartz fiber filters
99 (25 × 20 cm, Whatman) using a high-volume sampler (TH-1000H, Wuhan Tianhong; 1.05 m³/min). ~~Corn straw~~
100 ~~is recognized as a typical and common domestic biomass fuel in China, constituting approximately 40.0% of the~~
101 ~~total output from the agricultural products and has an estimated annual production of about 295 million tons.~~
102 ~~Therefore, PM_{2.5} emitted from corn straw combustion was selected as typical biomass burning aerosols in this~~
103 ~~work.~~ Figure S1 shows a schematic of sample collection process of biomass burning PM_{2.5} samples, and Table
104 S1 summarizes the concentrations of organic carbon (OC), element carbon (EC), the concentration of total
105 organic carbon (TOC) of each sample. This approach closely represents real-world biomass burning emissions
106 (Chen et al., 2019; Shan et al., 2017). For each sample, background aerosols were collected for 1 hour both
107 before to and after the sampling period.

108 ~~We selected five Atmospheric atmospheric~~ PM_{2.5} samples ~~were~~ collected at Peking University Changping
109 Campus (40°8'N, 116°6'E) from 15 December 2020 to 15 January 2021 ~~to extract p-BrC.~~ ~~Table S2 summarizes~~
110 ~~the sampling time and average PM_{2.5} mass concentrations during sampling of each sample. All samples were~~

111 ~~collected~~ using a high-volume sampler with the flow rate of 1.05 m³/min. ~~The sampling period of each sample~~
112 ~~was 23 hours.~~ Gaseous pollutants, PM_{2.5} mass concentrations, non-refractory submicron particles (NR-PM₁)
113 chemical composition, and meteorology were monitored (Figure S2; details in Table S3~~2~~).

114 For those PM_{2.5} samples, twenty 1.5-cm² filter sections were ultrasonically extracted in LC-MS grade
115 methanol (Merck Inc.) for twice (20 min) to extract p-BrC and b-BrC. Extracts were dried gentle stream of
116 ultrapure N₂ (>99.99%) and redissolved in ultrapure water.

117 2.2 Laboratory aqueous-phase photochemical aging setup

118 Photochemical aging experiments were conducted in a temperature-controlled (20 ± 0.1 °C) chamber,
119 equipped with 20 UV bulbs (40 W; λ_{max} = 370 nm). The TOC of all BrC solutions were adjusted to 50 mgC/L.
120 BrC solutions were irradiated in quartz bottles (10 mL) with added H₂O₂ (30 wt%, Aladdin) to generate OH
121 radicals. Steady-state OH concentrations ([OH]_{ss}) were quantified via pseudo-first-order decay of benzoic acid
122 (methods detailed in Text S1) (Hems and Abbatt, 2018). The average [OH]_{ss} was (3.17 ± 0.47) × 10⁻¹⁴ mol/L,
123 slightly below typical cloud water maxima~~-.~~

124 The transition from laboratory experimental illumination to actual solar radiation was applied by calculating
125 the ratio between laboratory and actual spectral flux densities following the identical calculation approach used
126 in our previous study (Qiu et al., 2024). Briefly, the scaling factor can be approximated as the ratio between the
127 integrated spectral flux densities of two different light sources. ~~Laboratory irradiation times were converted to~~
128 equivalent solar durations using a spectral flux density ratio~~he~~ the spectral flux densities of the UV bulbs used in
129 this work and the 24-hour average Beijing solar spectrum at 300 m above sea level were integrated from 360 nm
130 to 380 nm (see Text S2 for detail). The 24-hour average Beijing solar spectrum was simulated using the
131 Tropospheric Ultraviolet and Visible Radiation model (Table S4), and Figure S3 shows the comparison between
132 calculated and measured radiation spectrum. ~~The calculated~~ scaling factor~~:-~~ in this work is 3.86 (Qiu et al.,
133 2024) (Qiu et al., 2024). Samples were collected at 0, 2, 4, 8, and 16 hours of equivalent solar radiation.

134 Furthermore, a series of control experiments were performed under H₂O₂ free and dark conditions. In both
135 cases, the same BrC solutions (50 mgC/L TOC) were used for different types of BrC. The former consisted of
136 16 hours of radiation in the absence of H₂O₂. The dark experiments involved storing the solutions in complete
137 darkness for an identical period (16 hours) to account for any non-photochemical changes.

138 These experiments were configured to delineate the contributions of different pathways to BrC
139 photobleaching. The H₂O₂ added photochemical aging experiments elucidates the synergistic effect of OH
140 oxidation, direct BrC photolysis, and other light-independent reactions occur in dark conditions. The H₂O₂ free
141 experiments considered the sole contribution of the direct photolytic pathway. In addition, the dark control
142 experiments served to investigate any potential influence of chemical reactions in dark conditions on the BrC's
143 light-absorption capacity.

144 2.3 Light-absorption properties and molecular composition analysis of BrC

145 UV-Vis absorption spectra (250–700 nm) were recorded using a spectrophotometer (UV-1780, Shimadzu

146 Inc.). MAC normalized absorption to TOC concentrations. In eq.(1), $A_{10}^{abs}(\lambda)$, b, and c denotes the measured
147 base-10 absorbance, optical path length (1 cm), and measured TOC, respectively.

$$148 \quad \text{MAC}(\lambda) = \frac{A_{10}^{abs}(\lambda) \times \ln(10)}{b \times c} \quad (1)$$

149 BrC's molecular composition was analyzed via HRMS (Orbitrap Fusion™ Tribrid™, Thermo Scientific)
150 with electrospray ionization (ESI) in negative mode (ESI(-); m/z 70–700). Samples were directly injected into
151 HRMS at a flow rate of 10 $\mu\text{L}/\text{min}$. Triplicate analyses ensured reproducibility, with only peaks detected in all
152 replicates retained for assignment. Molecular formulas ($\text{C}_x\text{H}_y\text{O}_z\text{N}_w\text{S}_n$; $x = 1-90$, $y = 1-200$, $z = 0-20$, $w = 0-3$,
153 $n = 0-1$) were assigned with m/z error lower than ± 0.005 Da. The H/C, O/C, N/C, and S/C atom ratios for each
154 assigned formula were constrained to 0.3–3.0, 0–3.0, 0–0.5, and 0–2.0, respectively (Wang et al., 2017). Signal-
155 intensity-weighted average elemental compositions (eq.(2)), O/C atom ratios, and N/C atom ratios (eq.(3)) were
156 calculated as:

$$157 \quad Y = \frac{\sum_i x_i Y_i}{\sum_i x_i}, \text{ where } Y = \text{C, H, O, N, and S} \quad (2)$$

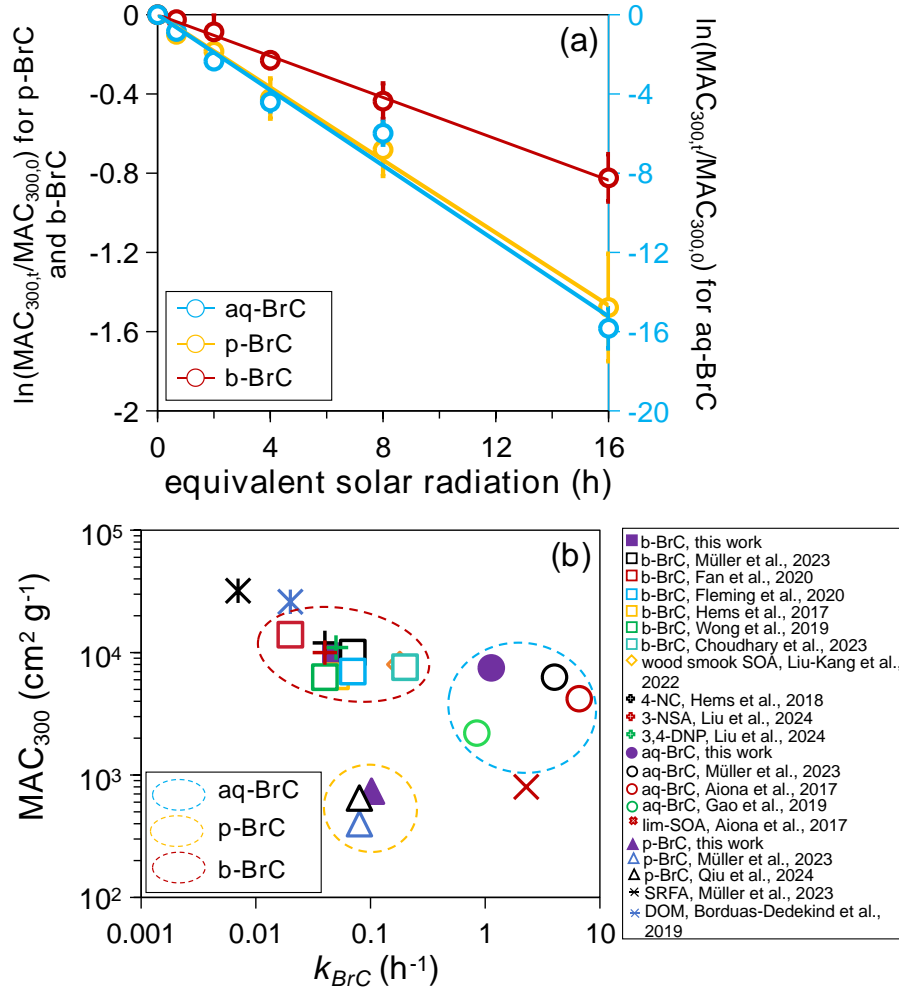
$$158 \quad Y/Z = \frac{\sum_i x_i Y_i}{\sum_i x_i Z_i}, \text{ where } Y/Z = \text{O/C or N/C} \quad (3)$$

159 where x_i in eqs. (2) and (3) indicated the signal-intensity-weighted factor.

160 **3. Results and Discussion**

161 **3.1 Quantification and Comparison of BrC Photobleaching Rates**

162 Given that BrC's light-absorption properties at shorter wavelengths are a better indicator of its
163 photobleaching kinetics (Aiona et al., 2017), we focused our analysis on the variation in the MAC at 300 nm
164 (MAC_{300}). The measured MAC_{300} of aq-BrC, p-BrC, and b-BrC is $(7.32 \pm 0.89) \times 10^3 \text{ cm}^2 \text{ g}^{-1}$, $(7.38 \pm 0.83) \times$
165 $10^2 \text{ cm}^2 \text{ g}^{-1}$, and $(9.44 \pm 0.71) \times 10^3 \text{ cm}^2 \text{ g}^{-1}$, respectively. Figure 1(a) shows the overall decay of MAC_{300} for
166 different BrC types, plotted as the natural logarithm of the ratio ($\ln(\text{MAC}_{300,t}/\text{MAC}_{300,0})$) versus irradiation hours.
167 The left axis of Figure 1(a) shows the variation in $\ln(\text{MAC}_{300,t}/\text{MAC}_{300,0})$ for p-BrC and b-BrC, while the right
168 axis denotes this variation for aq-BrC. Here, $\text{MAC}_{300,t}$ and $\text{MAC}_{300,0}$ denote the MAC_{300} after t hours of
169 irradiation and its initial value, respectively. The observed linear decay demonstrates that BrC undergoes
170 photobleaching regardless of its source. The aq-BrC has been almost completely bleached in the initial 2 hours.
171 The MAC_{300} decreased by 77.2% after 16 hours of radiation. In comparison, for b-BrC, the MAC_{300} only
172 decreased by 56.1%. Even after extending to 32 hours of radiation, b-BrC still kept strong light-absorption
173 capacity (see Figure S34). The differences in the variation in MAC_{300} for different types of BrC demonstrate that
174 aq-BrC undergoes rapid photobleaching in the presence of solar radiation, while b-BrC exhibits stable light-
175 absorption capacity during photobleaching.



176
 177 **Figure 1** (a) Variations in the $\ln(\text{MAC}_{300,t}/\text{MAC}_{300,0})$ of aq-BrC (blue plots, right axis), p-BrC (yellow plots, left
 178 axis), and b-BrC (red plots, left axis) as a function of radiation hours. Blue, yellow, and red lines indicate fitted
 179 k_{BrC} of aq-BrC, p-BrC, and b-BrC. Error bars represent one standard deviation of datapoints derive from three
 180 (aq-BrC and b-BrC) or five (p-BrC) parallel experiments. (b) The relationship between MAC_{300} and calculated
 181 k_{BrC} of different types of BrC in this work and other studies. 4-NC, 3-NSA, 3,4-DNP, SRFA, and DOM represents
 182 4-nitrocateol, 3-mitrosalicylic acid, 3,4-dinitrophenol, Suwannee River fulvic acid standard, and dissolved
 183 organic matters, respectively. Blue, yellow, and red circles marked aq-BrC (including BrC generated via
 184 aldehyde-amine condensation reactions), p-BrC, and b-BrC (including representative compounds emitted from
 185 biomass burning). The exact MAC_{300} values are obtained from figures in corresponding literatures, and k_{BrC} are
 186 calculated based on the MAC_{300} and hours of radiation.

187 The liner decline in $\ln(\text{MAC}_{300,t}/\text{MAC}_{300,0})$ indicates that BrC photobleaching fitted the pseudo-first order
 188 kinetic, which was represented by the negative slope of $\ln(\text{MAC}_{300,t}/\text{MAC}_{300,0})$ vs. radiation hours:

189
$$\text{MAC}_{300,t} = \text{MAC}_{300,0} \times \exp(-k_{BrC}t) \quad (4)$$

190 where k_{BrC} is the overall photobleaching rate constant. The calculated k_{BrC} of aq-BrC, p-BrC, and b-BrC were
 191 $(1.13 \pm 0.08) \text{ hour}^{-1}$, $(0.12 \pm 0.02) \text{ hour}^{-1}$, and $(0.05 \pm 0.01) \text{ hour}^{-1}$, respectively. Correspondingly, the lifetime of

192 BrC (τ_{BrC} , indicated by BrC's absorption decreased to 1/e of its initial value) (Schnitzler et al., 2022) were 1.05
193 hours, 10.91 hours, and 19.16 hours, respectively. Longer τ_{BrC} of b-BrC indicates its absorption largely retains
194 during atmospheric transportation process. This order-of-magnitude difference in k_{BrC} among three BrC types,
195 quantified under comparable conditions, highlights a fundamental source dependency that cannot be attributed
196 to environmental condition variability. This clear difference necessitates a molecular-level explanation, which
197 we pursue by examining the dominant bleaching pathway and the underlying chemical composition.

198 Figure 1(b) presents a comparison of MAC_{300} versus overall k_{BrC} for BrC from various sources, including
199 data from this study and other studies (data and references in Table S3S5). Based on their sources, we classified
200 aq-BrC (including BrC generated via aldehyde-amine condensation reactions), p-BrC, and b-BrC (including
201 representative compounds emitted from biomass burning) in three different clusters. Our results are comparable
202 to those of previous studies. The characteristic of aq-BrC is strong absorption, rapid photobleaching. This
203 demonstrates that the light-absorption capacity of BrC generated by secondary atmospheric aqueous phase
204 reactions (De Haan et al., 2017) decrease rapidly in the presence of solar radiation. In stark contrast, b-BrC
205 shows strong absorption but slow photobleaching, implying its stable strong absorption in the atmosphere. p-
206 BrC exhibits weak absorption and slow photobleaching, which has also been observed in different urban areas,
207 including Eastern China (Qiu et al., 2024), India (Dasari et al., 2019), Northern Europe (Müller et al., 2023), and
208 the United States (Chen et al., 2021). It is noteworthy that p-BrC contains a mixture of primary and secondary
209 BrC that is challenging to separate quantitatively. However, from molecular composition and solar radiation
210 during sampling, p-BrC is considered to be predominantly of primary emissions. Herein, we further analyzed
211 the molecular composition of p-BrC following the non-target analysis approach used in our previous study (Qiu
212 et al., 2024), more details were described in Text S3. Figure S5 shows the molecular composition and relevant
213 solar radiation during sampling, which is represented by the 75th percentile solar radiation (Rad_{75}). Low Rad_{75}
214 showed limited photochemical aging prior to analysis, and high mass fraction of nitrophenols proved the
215 dominate role of primary emission for p-BrC.

216 Having investigated the differences in overall photobleaching rates across different BrC types, we further
217 elucidated the underlying mechanisms by assessing the contribution of each photobleaching pathway. Previous
218 studies suggest that BrC photobleaching occurs via three different pathways, including direct photolysis, OH
219 oxidation, and other light-independent reactions occur in dark conditions (Gao and Zhang, 2019; Liu-Kang et
220 al., 2022; Wong et al., 2019). Choudhary et al. (2023) (Choudhary et al., 2023) have demonstrated that in the
221 presence of H_2O_2 , the overall k_{BrC} can be expressed as a linear sum of the pseudo first-order effective
222 photobleaching rate constant due to OH oxidation ($k_{BrC,OH}$), BrC direct photolysis ($k_{BrC,pho}$), and other light-
223 independent reactions occur in dark conditions ($k_{BrC,ctrl}$), see eq. (5):

$$224 \quad k_{BrC} = k_{BrC,OH} + k_{BrC,pho} + k_{BrC,ctrl} \quad (5)$$

225 The $k_{BrC,pho}$ and $k_{BrC,ctrl}$ are derived from the pseudo-first-order decay of MAC_{300} in H_2O_2 free experiments
226 and dark control experiments, respectively, using the calculation approach identical to eq. (4) and the
227 experimental procedures detailed in Section 2.2. Therefore, although $k_{BrC,OH}$ cannot be measured directly, it can
228 be indirectly determined by calculating the difference between the overall k_{BrC} and the sum of $k_{BrC,pho}$ (from H_2O_2
229 free experiments) and $k_{BrC,ctrl}$ (from dark control experiments).

230

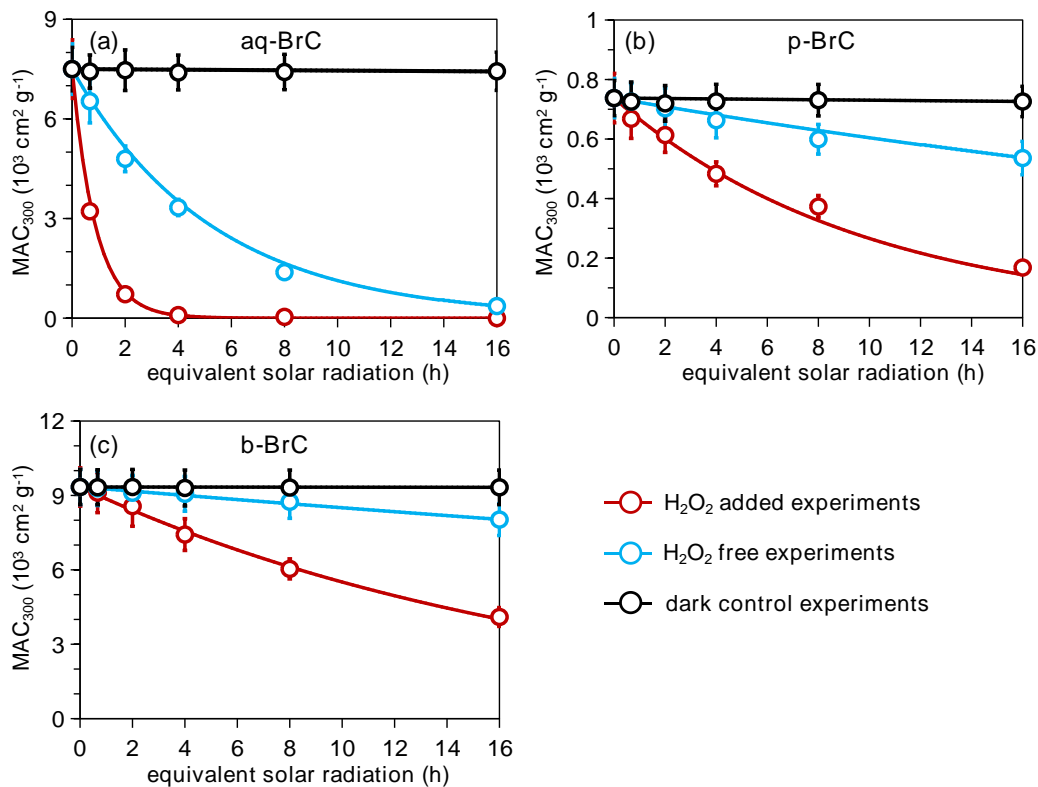
Table 1 The $k_{BrC,ctrl}$, $k_{BrC,pho}$, and $k_{BrC,OH}$ for different BrC types

BrC type	$k_{BrC,ctrl}$	$k_{BrC,pho}$	$k_{BrC,OH}$
aq-BrC	$(0.004 \pm 0.002) \text{ h}^{-1}$	$(0.19 \pm 0.03) \text{ h}^{-1}$	$(0.94 \pm 0.06) \text{ h}^{-1}$
p-BrC	$(0.007 \pm 0.001) \text{ h}^{-1}$	$(0.02 \pm 0.005) \text{ h}^{-1}$	$(0.08 \pm 0.02) \text{ h}^{-1}$
b-BrC	$(0.006 \pm 0.002) \text{ h}^{-1}$	$(0.01 \pm 0.004) \text{ h}^{-1}$	$(0.04 \pm 0.01) \text{ h}^{-1}$

231 Figure 2 displays the variations in MAC₃₀₀ in photochemical aging experiments (with H₂O₂, red line,
 232 representing the synergistic effect of OH oxidation, direct BrC photolysis, and other light-independent reactions
 233 occur in dark conditions), H₂O₂ free experiments (blue line, representing the contribution of BrC direct
 234 photolysis), and dark control experiments (black line, representing the contribution of other light-independent
 235 reactions occur in dark conditions). It is noted that for dark control experiments, the x-axis denotes the time the
 236 BrC solution is kept under dark conditions. Table 1 summarizes the $k_{BrC,ctrl}$, $k_{BrC,pho}$, and $k_{BrC,OH}$ for different BrC
 237 types. Specifically, MAC₃₀₀ variations were negligible in dark controls, rendering the calculated $k_{BrC,ctrl}$ was close
 238 to 0. For all BrC types, $k_{BrC,pho}$ was substantially lower than $k_{BrC,OH}$. The overwhelming contribution of $k_{BrC,OH}$
 239 (over 80% of k_{BrC}) unambiguously identifies OH oxidation as the dominant mechanism governing BrC
 240 photobleaching. The dominate role of OH oxidation in BrC photobleaching have been also proved in several
 241 previous studies (Choudhary et al., 2023; Hems and Abbatt, 2018; Zhao et al., 2015), this work provide
 242 quantitative and comparative evidence regardless of BrC types. Consequently, the observed differences in k_{BrC}
 243 among different types of BrC can be fundamentally attributed to the molecular-composition-dependent reactivity
 244 of BrC components toward OH radicals. Hence, understanding the underlying molecular composition that
 245 determine a BrC molecule's susceptibility to this OH oxidation.

246 It is important to note that the laboratory-synthesized aq-BrC represents a simplified chemical system.
 247 While it provides a clear mechanistic understanding of rapid photobleaching driven by BrC chromophores with
 248 high chemical reactivity, real atmospheric aqueous-phase processes involve more complex precursors and
 249 mixtures, yielding secondary BrC with different photobleaching kinetics. Nevertheless, the dominate role of OH
 250 oxidation established in this work, which provides a critical lens through which to interpret the slower
 251 photobleaching rates of the more complex ambient (p-BrC) and biomass burning (b-BrC) samples. Specifically,
 252 the $k_{BrC,pho}$ was $(0.19 \pm 0.03) \text{ h}^{-1}$, $(0.02 \pm 0.005) \text{ h}^{-1}$, and $(0.01 \pm 0.004) \text{ h}^{-1}$ for aq-BrC, p-BrC, and b-BrC,
 253 respectively. The calculated $k_{BrC,OH}$ was $(0.94 \pm 0.06) \text{ h}^{-1}$, $(0.08 \pm 0.02) \text{ h}^{-1}$, and $(0.04 \pm 0.01) \text{ h}^{-1}$ for aq-BrC, p-BrC,
 254 and b-BrC.

255 ~~For all types of BrC, the overwhelming contribution of $k_{BrC,OH}$ (over 80% of k_{BrC}) unambiguously identifies~~
 256 ~~OH oxidation as the dominant mechanism governing BrC photobleaching. Consequently, the observed~~
 257 ~~differences in k_{BrC} among different types of BrC can be fundamentally attributed to the molecular composition-~~
 258 ~~dependent reactivity of BrC components toward OH radicals. Hence, understanding the underlying molecular~~
 259 ~~composition that determine a BrC molecule's susceptibility to this OH oxidation.~~



260

261 **Figure 2** The variations in MAC₃₀₀ in photochemical aging experiments (with H₂O₂, red line, representing the
 262 synergistic effect of OH oxidation, direct BrC photolysis, and other light-independent reactions occur in dark
 263 conditions), H₂O₂ free experiments (blue line, representing the variation in MAC₃₀₀ contributed by BrC direct
 264 photolysis), and dark control experiments (black line, representing the variation in MAC₃₀₀ contributed by other
 265 light-independent reactions occur in dark conditions) for (a) aq-BrC, (b) p-BrC, and (c) b-BrC, respectively. For
 266 dark control experiments (black line), the x-axis represents the time the BrC solution is kept in the absence of
 267 light.

268 3.2 Chemical investigation of different BrC photobleaching rates

269 To elucidating the differences in BrC photobleaching rates, we investigated BrC's molecular composition
 270 before and after photobleaching, which was represented by BrC's molecular composition after 16 hours of
 271 radiation.

272 Table 24 summarizes the signal-intensity-weighted average elemental compositions, molecular weights,
 273 O/C ratios, and N/C ratios of different types of BrC before and after 16 hours of radiation. The observed decrease
 274 in average molecular weights upon photobleaching across all BrC types, alongside an elevated O/C ratio, points
 275 to the production of more oxidized, lower-mass species. Additionally, we found the mass concentrations of low-
 276 molecular-weight organic acids (formic acid, acetic acid, and oxalic acid; see Figure S46) significantly increased
 277 with longer radiation hours, demonstrating carbon backbone fragmentation (Borduas-Dedekind et al., 2019).
 278 Figure S5-S7 demonstrates that more products with lower C atom numbers are detected after photobleaching,
 279 further proves the carbon backbone fragmentation. Considering OH oxidation dominates BrC photobleaching,

280 the molecular-level evolution aligns with OH-mediated degradation pathways (Hems et al., 2020; Qiu et al.,
281 2024; Liu et al., 2025): (i) electrophilic addition to unsaturated bonds (like C=C bonds) and (ii) subsequent
282 carbon backbone fragmentation.

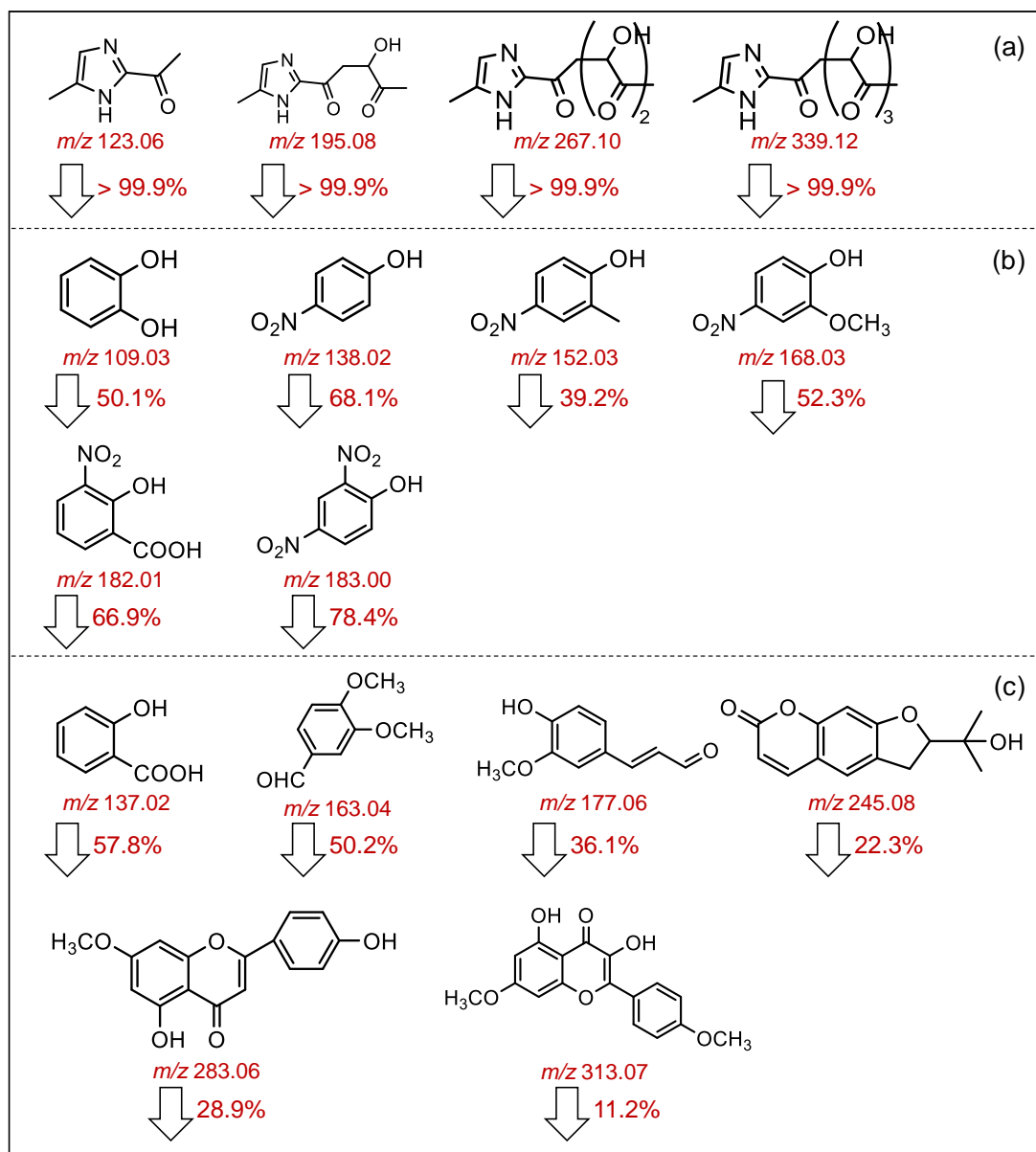
283 In addition, the reduced N/C atom ratios (Table 42) further confirmed degradation of N-containing
284 compounds, which are key UV-Vis absorbers contributing significantly to BrC absorption (Lin et al., 2017; Wang
285 et al., 2019; Zeng et al., 2021; Li et al., 2025). The formation of compounds with higher oxidation states and the
286 degradation of N-containing compounds reduce the conjugation degrees of BrC, diminishing $\pi \rightarrow \pi^*$ electronic
287 transitions and weakening light-absorption capacity.

288 **Table 42** Variations in the signal-intensity-weighted average elemental compositions, molecular weights,
289 O/C ratios, and N/C ratios of different types of BrC before and after photobleaching

aq-BrC	elemental composition	molecular weight	O/C	N/C
before	C _{8.94} H _{10.22} O _{4.64} N _{1.33}	210.36	0.52	0.15
after	C _{8.22} H _{10.17} O _{4.66} N _{1.07}	198.35	0.57	0.12
p-BrC	elemental composition	molecular weight	O/C	N/C
before	C _{7.88} H _{8.38} O _{2.47} N _{2.13} S _{0.65}	193.08	0.31	0.28
after	C _{7.21} H _{9.17} O _{2.52} N _{1.82} S _{0.68}	183.25	0.35	0.25
b-BrC	elemental composition	molecular weight	O/C	N/C
before	C _{15.92} H _{16.68} O _{6.05} N _{1.18} S _{0.31}	330.96	0.38	0.08
after	C _{15.42} H _{16.92} O _{6.11} N _{1.07} S _{0.41}	327.82	0.40	0.07

290 Subsequently, we determined representative BrC chromophores relate to the photobleaching of different
291 types of BrC based on the following three criteria. Firstly, we calculated the differential HRMS spectra of
292 different types of BrC before and after photobleaching (Figure S8). These peaks with negative intensities (> 3
293 times the signal-to-noise ratio) denote species consumed after photobleaching. Secondly, these candidate species
294 were cross-compared to identify compounds that were highly characteristic of each specific source. Lastly,
295 tandem HRMS (HRMS²) analysis was adopted to determine the chemical structure of selected BrC
296 chromophores.

297 Figure S6 shows the differential HRMS spectra, the negative peaks represent species consumed after
298 photobleaching. In this work, The the photooxidation of MG and imidazole-2-carboxaldehyde (2-IC) oligomers
299 (Aiona et al., 2017) with formula C_{3n}H_{4n}N₂O_{2n-3} (n = 2-5; including *m/z* 123.06, 195.08, 267.10, and 339.12),
300 phenols and nitrophenols (Hems and Abbatt, 2018; Magalhães et al., 2017) (including *m/z* 109.03, 138.02, 152.03,
301 168.03, 182.01, and 183.00), and lignin derivatives (Fleming et al., 2020) (including *m/z* 137.02, 163.04, 245.08,
302 283.06, and 313.07) were identified as the dominant reactions in the photobleaching of aq-BrC, p-BrC, and b-
303 BrC, respectively. Compounds identified as products after photobleaching for aq-BrC, p-BrC, and b-BrC are
304 respectively summarized in Tables S4S6-S68. It is acknowledged that secondary BrC comprises a wide variety
305 of compounds formed through different pathways. While phenols and nitrophenols identified here can
306 themselves be secondary products, their markedly slower photobleaching rate (compared to the MG/AS-derived
307 aq-BrC in this work) highlights the substantial kinetic diversity within the broader secondary BrC. This further
308 reinforces that the molecular architecture, rather than the primary or secondary classification, is the fundamental



310

311 **Figure 3** The chemical structures of (a) MG and 2-IC oligomers detected in aq-BrC; (b) phenols and nitrophenols
 312 detected in p-BrC, and (c) lignin derivatives detected in b-BrC. The detected m/z for these compounds are marked
 313 under their structures. The ratios of decline in signal intensities for these compounds after 16 hours of radiation
 314 are indicated next to the bottom arrows.

315 Figure 3 displays the chemical structures of these MG and 2-IC oligomers, phenols and nitrophenols, and
 316 lignin derivatives, as well as the declines in their signal intensities after 16 hours of radiation. Variations in
 317 HRMS signal intensities represent the changes in the mass concentrations, though specific mass concentrations
 318 cannot be derived. Figure 3(a) illustrates the predominant molecular species and the corresponding decline in
 319 MG and 2-IC oligomers during the photobleaching of aq-BrC. Following photobleaching, these oligomers

320 became undetectable (signal-to-noise ratio < 3), experiencing a reduction in signal intensity of >99.9% (Figure
321 3(a)). This observation is consistent with the nearly complete bleaching of aq-BrC. The high reactivity of the
322 chain structures of MG and 2-IC oligomers with OH radicals (Aiona et al., 2017) explains the elevated k_{BrC} value
323 observed for aq-BrC.

324 As shown in Figure 3(b), a greater number of electron-withdrawing substituents on the benzene ring
325 correlates with a more significant decline of signal intensity after photobleaching. For instance, 2-methyl-4-
326 nitrophenol (m/z 152.03), which bears an electron-donating methyl group in addition to the electron-withdrawing
327 nitro substituent present in 4-nitrophenol (m/z 138.02), demonstrates a comparatively lower signal attenuation
328 of 39.2% after photobleaching, whereas 4-nitrophenol exhibits a signal decrease of 68.1%. The electron-
329 withdrawing substituents exert both inductive and resonance effects, effectively diminishing the electron density
330 of the π -system of the aromatic ring. This electron-deficient state enhances the susceptibility of these species to
331 nucleophilic attack by OH radicals, thereby facilitating their photooxidation and contributing to the observed
332 photobleaching behavior. However, the reactivity of these species remains lower than that of MG and 2-IC
333 oligomers, which explains lower k_{BrC} for p-BrC compares to aq-BrC.

334 In comparison, the signal intensities of the majority of lignin derivatives only decreased by below 50%,
335 corresponding to the lowest k_{BrC} for b-BrC (Figure 3(c)). Specifically, nodakenetin and flavonoids (m/z 245.08,
336 283.06, and 313.07) exhibit highly stabilized molecular structures, wherein the aromatic rings conjugated with
337 oxygen-containing heterocyclic moieties significantly reduce their chemical reactivity, resulting in low k_{BrC} for
338 b-BrC. The chemical stability of lignin derivatives has been also proved by previous laboratory experiment
339 (Wong et al., 2019). However, studies found that levoglucosan, which is an important component in biomass
340 burning aerosols, may be oxidized by OH radicals and therefore slow down the reaction of other BrC
341 chromophores reacting with OH (Bai et al., 2013; Zhao et al., 2014). In this work, the same TOC mass
342 concentrations (50 mg/L) across all BrC types provides equal total potential OH sinks, making the observed
343 order-of-magnitude difference in k_{BrC} more likely attributable to the reactivity of the chromophores themselves
344 rather than solely to differences in competitor abundance. Additionally, the identified lignin derivatives exhibited
345 low signal decay percentages despite being exposed to the same $[OH]_{ss}$ as the highly reactive BrC chromophores.
346 Hence, it is expected that the chemical stability of lignin derivative leads to the low k_{BrC} for b-BrC.

347 We noted that the exact variation in the mass concentration of compounds shown in Figure 3 were not
348 derived in this work. Ultra-high performance liquid chromatography (UHPLC)-HRMS analysis using standards
349 or surrogate standards should be adopted to obtain the mass concentration of these compounds. However, this
350 work aims to comparatively track the changes in molecular composition for each specific BrC type before and
351 after photobleaching. While absolute quantification is not feasible based on HRMS analysis, the relative changes
352 in signal intensity for a given compound are comparable within the same sample matrix. Therefore, the variation
353 in signal intensity for a specific m/z can be reliably interpreted as a corresponding change in its relative mass
354 concentration.

355 In addition, while the species highlighted in Figure 3 were rigorously selected as representative and reactive
356 chromophores through the differential screening and structural identification process described above, we fully
357 acknowledge that our analysis may not capture all potential BrC chromophores. Limitations in analytical

358 sensitivity, chromatographic separation, and the chemical complexity of BrC result in several BrC chromophores,
359 particularly those at low concentrations or with poor ionization efficiency, might not be detected or their changes
360 fully characterized. Therefore, while the reported decay percentages for the identified species are robust, the
361 total BrC photobleaching likely involves contributions from additional chromophores not specifically tracked
362 here.

363 **4. Conclusion and Atmospheric Implication**

364 This work quantifies the k_{BrC} for three different types of BrC and demonstrates that their order-of-magnitude
365 differences (aq-BrC > p-BrC > b-BrC) originate from distinct molecular susceptibilities to OH-driven oxidation
366 through controlled comparative experiments. While the source dependency of BrC photobleaching has been
367 suggested, our study mechanistically establishes the linkage between BrC photobleaching kinetics and molecular
368 composition. Specifically, rapid photobleaching of aq-BrC is governed by the high OH reactivity of MG and 2-
369 IC oligomers; in comparison, the remarkable stability of b-BrC is attributed to resilient, conjugated aromatic
370 systems in lignin derivatives. For p-BrC, an intermediate k_{BrC} was observed, consistent with the oxidation
371 kinetics of nitrophenolic chromophores. Critically, we show that OH oxidation accounts for >80% of the total
372 photobleaching across all sources, identifying it as the dominant and unifying chemical pathway under aqueous
373 conditions.

374 ~~This work demonstrates that BrC exhibits source-dependent photobleaching rates. Specifically, aq-BrC~~
375 ~~shows the highest k_{BrC} , followed by p-BrC and b-BrC, indicating that light absorption capacity of b-BrC keep~~
376 ~~stable during photobleaching. In addition, considering the overwhelming contribution of $k_{BrC,OH}$ to k_{BrC} , the OH~~
377 ~~oxidation is determined as the predominate pathway of BrC photobleaching. The OH oxidation leads to the~~
378 ~~formation of compounds with higher oxidation state and lower molecular weights, which decreases the~~
379 ~~conjugation degree of BrC and therefore results in photobleaching. The oxidation of MG and 2-IC oligomers,~~
380 ~~phenols and nitrophenols, and lignin derivatives dominate the photobleaching of aq-BrC, p-BrC, and b-BrC,~~
381 ~~respectively.~~

382 These quantified, ~~Source~~source-dependent k_{BrC} values and their molecular-level ~~changes~~ emphasizes the
383 necessitate explicit consideration of source variability when evaluating BrC's ~~climate effect~~radiative effect.
384 Current models often assume constant k_{BrC} based on simplified representative compounds or field data (Hems
385 and Abbatt, 2018; Schnitzler et al., 2022; Wang et al., 2018), yet substantial discrepancies exist. For instance,
386 the reported k_{BrC} values differ by approximately an order of magnitude between field observations and laboratory
387 simulations (Schnitzler et al., 2022; Wang et al., 2018). Spatiotemporal heterogeneity in BrC sources (Xiong et
388 al., 2022) (fossil fuel/biomass combustion, secondary formation) drives global regional variations in k_{BrC} . We
389 should acknowledge that though source-dependent BrC photobleaching rates are essential in assessing BrC's
390 global DRE, the impact of environmental conditions like temperature and relative humidity are also decisive
391 (Schnitzler et al., 2022).

392 ~~To further reduce the uncertainties in assessing BrC's global DRE, it is imperative to systematically quantify~~
393 ~~the impact of BrC's source and integrate source-dependent data into regional and global climate models.~~

394 In addition, the low k_{BrC} for b-BrC explains unexpectedly high BrC absorption in remote regions (e.g., the
395 Arctic). Field data confirm biomass burning contributes 57% of Arctic BrC while < 10% for secondary BrC (Yue
396 et al., 2022). Previous studies have confirmed that biomass burning aerosols contains substantial amounts of
397 lignin derivatives (Wong et al., 2019), which exhibit strong light-absorbing properties and chemical stability in
398 OH oxidation. Therefore, during the long-range transport (Zhang et al., 2025), b-BrC is expected to retain strong
399 absorption, leading to enhancement of the aerosol DRE over large spatial scales. On a global scale, one major
400 source of b-BrC is wildfire events (Wang et al., 2025; Shen et al., 2024; Bond et al., 2004). With the increasing
401 frequency of wildfires (Yue et al., 2013; Hurteau et al., 2014; Cunningham et al., 2024; Jain et al., 2022), the
402 emission of b-BrC is expected to rise correspondingly. In all, b-BrC would exert a significant influence on BrC's
403 global radiative effect.

404 **Associate Content**

405 **Code and Data Availability**

406 The data used in this study is available upon request from the corresponding author (zhijunwu@pku.edu.cn).

407 **Author Contributions**

408 Y.Q. and Z.W. designed this work. Y.Q., T.Q., Y.G., and D.L. collected and analyzed the measurement data.
409 Y.Q., T.Q., Y.L., and R.M. analyzed UHPLC-MS data. Z.W. and M.H. edited the manuscript. All authors have
410 read and agreed to submit this manuscript.

411 **Funding**

412 This work is funded by National Natural Science Foundation of China – Youth Program (42507137), China
413 Postdoctoral Science Foundation (2025M771267), and the National Key Research and Development Program
414 of China (2022YFC3701000, Task 4).

415 **Competing Interests**

416 The authors declare that they have no conflict of interest.

417 **Acknowledgements**

418 This research has been supported by the National Natural Science Foundation of China (grant no.
419 42507137), Chinese Postdoctoral Science Foundation (grant no. 2025M771267), the National Key Research and
420 Development Program of China (grant no. 2022YFC3701000, Task 4).

421

422 **References**

- 423 Aiona, P. K., Lee, H. J., Leslie, R., Lin, P., Laskin, A., Laskin, J., Nizkorodov, S. A.: Photochemistry of Products
424 of the Aqueous Reaction of Methylglyoxal with Ammonium Sulfate. *ACS Earth and Space Chemistry*. 1, 522-532.
425 <https://doi.org/10.1021/acsearthspacechem.7b00075>, 2017.
- 426 Bai, J., Sun, X., Zhang, C., Xu, Y., Qi, C.: The OH-initiated atmospheric reaction mechanism and kinetics for
427 levoglucosan emitted in biomass burning. *Chemosphere*. 93, 2004-2010.
428 <https://doi.org/10.1016/j.chemosphere.2013.07.021>, 2013.
- 429 Bond, T. C.: Spectral dependence of visible light absorption by carbonaceous particles emitted from coal
430 combustion. *Geophysical Research Letters*. 28, 4075-4078. <https://doi.org/10.1029/2001GL013652>, 2001.
- 431 Bond, T. C., Streets, D. G., Yarber, K. F., Nelson, S. M., Woo, J.-H., Klimont, Z.: A technology-based global
432 inventory of black and organic carbon emissions from combustion. *Journal of Geophysical Research: Atmospheres*.
433 109. <https://doi.org/10.1029/2003JD003697>, 2004.
- 434 Borduas-Dedekind, N., Ossola, R., David, R. O., Boynton, L. S., Weichlinger, V., Kanji, Z. A., McNeill, K.:
435 Photomineralization mechanism changes the ability of dissolved organic matter to activate cloud droplets and to
436 nucleate ice crystals. *Atmospheric Chemistry and Physics*. 19, 12397-12412. [https://doi.org/10.5194/acp-19-12397-](https://doi.org/10.5194/acp-19-12397-2019)
437 [2019](https://doi.org/10.5194/acp-19-12397-2019), 2019.
- 438 Brown, H., Liu, X., Pokhrel, R., Murphy, S., Lu, Z., Saleh, R., Mielonen, T., Kokkola, H., Bergman, T., Myhre,
439 G., Skeie, R. B., Watson-Paris, D., Stier, P., Johnson, B., Bellouin, N., Schulz, M., Vakkari, V., Beukes, J. P., van Zyl,
440 P. G., Liu, S., Chand, D.: Biomass burning aerosols in most climate models are too absorbing. *Nature Communications*.
441 12, 277. <https://doi.org/10.1038/s41467-020-20482-9>, 2021.
- 442 Chen, L.-W. A., Chow, J. C., Wang, X., Cao, J., Mao, J., Watson, J. G.: Brownness of Organic Aerosol over the
443 United States: Evidence for Seasonal Biomass Burning and Photobleaching Effects. *Environmental Science &*
444 *Technology*. 55, 8561-8572. <https://doi.org/10.1021/acs.est.0c08706>, 2021.
- 445 Chen, Q., Sun, H., Wang, J., Shan, M., Yang, X., Deng, M., Wang, Y., Zhang, L.: Long-life type — The dominant
446 fraction of EPFRs in combustion sources and ambient fine particles in Xi'an. *Atmos. Environ.* 219, 117059.
447 <https://doi.org/10.1016/j.atmosenv.2019.117059>, 2019.
- 448 Choudhary, V., Roson, M. L., Guo, X., Gautam, T., Gupta, T., Zhao, R.: Aqueous-phase photochemical oxidation
449 of water-soluble brown carbon aerosols arising from solid biomass fuel burning. *Environmental Science: Atmospheres*.
450 3, 816-829. <https://doi.org/10.1039/D2EA00151A>, 2023.
- 451 Chung, C. E., Ramanathan, V., Decremier, D.: Observationally constrained estimates of carbonaceous aerosol
452 radiative forcing. *Proceedings of the National Academy of Sciences USA*. 109, 11624-11629.
453 <https://doi.org/10.1073/pnas.1203707109>, 2012.
- 454 Corr, C. A., Hall, S. R., Ullmann, K., Anderson, B. E., Beyersdorf, A. J., Thornhill, K. L., Cubison, M. J., Jimenez,
455 J. L., Wisthaler, A., Dibb, J. E.: Spectral absorption of biomass burning aerosol determined from retrieved single

456 scattering albedo during ARCTAS. *Atmospheric Chemistry and Physics*. 12, 10505-10518.
457 <https://doi.org/10.5194/acp-12-10505-2012>, 2012.

458 Cunningham, C. X., Williamson, G. J., Bowman, D. M. J. S.: Increasing frequency and intensity of the most
459 extreme wildfires on Earth. *Nature Ecology & Evolution*. 8, 1420-1425. <https://doi.org/10.1038/s41559-024-02452-2>,
460 2024.

461 Dalton, A. B., Nizkorodov, S. A.: Photochemical Degradation of 4-Nitrocatechol and 2,4-Dinitrophenol in a
462 Sugar-Glass Secondary Organic Aerosol Surrogate. *Environmental Science & Technology*. 55, 14586-14594.
463 <https://doi.org/10.1021/acs.est.1c04975>, 2021.

464 Dasari, S., Andersson, A., Bikkina, S., Holmstrand, H., Budhavant, K., Satheesh, S., Asmi, E., Kesti, J., Backman,
465 J., Salam, A., Bisht, D. S., Tiwari, S., Hameed, Z., Gustafsson, Ö.: Photochemical degradation affects the light
466 absorption of water-soluble brown carbon in the South Asian outflow. *Science Advances*. 5, eaau8066.
467 <https://doi.org/10.1126/sciadv.aau8066>, 2019.

468 De Haan, D. O., Hawkins, L. N., Welsh, H. G., Pednekar, R., Casar, J. R., Pennington, E. A., de Loera, A., Jimenez,
469 N. G., Symons, M. A., Zauscher, M., Pajunoja, A., Caponi, L., Cazaunau, M., Formenti, P., Gratién, A., Panguí, E.,
470 Doussin, J.-F.: Brown Carbon Production in Ammonium- or Amine-Containing Aerosol Particles by Reactive Uptake
471 of Methylglyoxal and Photolytic Cloud Cycling. *Environmental Science & Technology*. 51, 7458-7466.
472 <https://doi.org/10.1021/acs.est.7b00159>, 2017.

473 Fan, X., Yu, X., Wang, Y., Xiao, X., Li, F., Xie, Y., Wei, S., Song, J., Peng, P. a.: The aging behaviors of
474 chromophoric biomass burning brown carbon during dark aqueous hydroxyl radical oxidation processes in laboratory
475 studies. *Atmospheric Environment*. 205, 9-18. <https://doi.org/10.1016/j.atmosenv.2019.02.039>, 2019.

476 Fleming, L. T., Ali, N. N., Blair, S. L., Roveretto, M., George, C., Nizkorodov, S. A.: Formation of Light-
477 Absorbing Organosulfates during Evaporation of Secondary Organic Material Extracts in the Presence of Sulfuric
478 Acid. *ACS Earth and Space Chemistry*. 3, 947-957. <https://doi.org/10.1021/acsearthspacechem.9b00036>, 2019.

479 Fleming, L. T., Lin, P., Roberts, J. M., Selimovic, V., Yokelson, R., Laskin, J., Laskin, A., Nizkorodov, S. A.:
480 Molecular composition and photochemical lifetimes of brown carbon chromophores in biomass burning organic
481 aerosol. *Atmospheric Chemistry and Physics*. 20, 1105-1129. <https://doi.org/10.5194/acp-20-1105-2020>, 2020.

482 Fu, T.-M., Jacob, D. J., Wittrock, F., Burrows, J. P., Vrekoussis, M., Henze, D. K.: Global budgets of atmospheric
483 glyoxal and methylglyoxal, and implications for formation of secondary organic aerosols. *Journal of Geophysical
484 Research: Atmospheres*. 113. <https://doi.org/10.1029/2007JD009505>, 2008.

485 Gao, Y., Zhang, Y.: Optical properties investigation of the reactions between methylglyoxal and
486 glycine/ammonium sulfate. *Spectrochimica Acta Part A: Molecular and Biomolecular Spectroscopy*. 215, 112-121.
487 <https://doi.org/10.1016/j.saa.2019.02.087>, 2019.

488 Gu, J., Dutta, S., Sioud, S., Go, B. R., Maity, B., Cavallo, L., Zhang, R., Chan, C. K.: Photoinduced
489 Transformation in Glyoxal- and Methylglyoxal-Ammonium Solutions: Role of Photolysis and Photosensitization.
490 *Environmental Science & Technology*. 59, 16628-16640. <https://doi.org/10.1021/acs.est.5c04889>, 2025.

491 Heald, C. L., Ridley, D. A., Kroll, J. H., Barrett, S. R. H., Cady-Pereira, K. E., Alvarado, M. J., Holmes, C. D.:
492 Contrasting the direct radiative effect and direct radiative forcing of aerosols. *Atmospheric Chemistry and Physics*. 14,
493 5513-5527. <https://doi.org/10.5194/acp-14-5513-2014>, 2014.

494 Hems, R. F., Abbatt, J. P. D.: Aqueous Phase Photo-oxidation of Brown Carbon Nitrophenols: Reaction Kinetics,
495 Mechanism, and Evolution of Light Absorption. *ACS Earth and Space Chemistry*. 2, 225-234.
496 <https://doi.org/10.1021/acsearthspacechem.7b00123>, 2018.

497 Hems, R. F., Schnitzler, E. G., Bastawrous, M., Soong, R., Simpson, A. J., Abbatt, J. P. D.: Aqueous
498 Photoreactions of Wood Smoke Brown Carbon. *ACS Earth and Space Chemistry*. 4, 1149-1160.
499 <https://doi.org/10.1021/acsearthspacechem.0c00117>, 2020.

500 Hems, R. F., Schnitzler, E. G., Liu-Kang, C., Cappa, C. D., Abbatt, J. P. D.: Aging of Atmospheric Brown Carbon
501 Aerosol. *ACS Earth and Space Chemistry*. 5, 722-748. <https://doi.org/10.1021/acsearthspacechem.0c00346>, 2021.

502 Hurteau, M. D., Westerling, A. L., Wiedinmyer, C., Bryant, B. P.: Projected Effects of Climate and Development
503 on California Wildfire Emissions through 2100. *Environmental Science & Technology*. 48, 2298-2304.
504 <https://doi.org/10.1021/es4050133>, 2014.

505 Jain, P., Castellanos-Acuna, D., Coogan, S. C. P., Abatzoglou, J. T., Flannigan, M. D.: Observed increases in
506 extreme fire weather driven by atmospheric humidity and temperature. *Nature Climate Change*. 12, 63-70.
507 <https://doi.org/10.1038/s41558-021-01224-1>, 2022.

508 Jo, D. S., Park, R. J., Lee, S., Kim, S. W., Zhang, X.: A global simulation of brown carbon: implications for
509 photochemistry and direct radiative effect. *Atmospheric Chemistry and Physics*. 16, 3413-3432.
510 <https://doi.org/10.5194/acp-16-3413-2016>, 2016.

511 Kirchstetter, T. W., Novakov, T., Hobbs, P. V.: Evidence that the spectral dependence of light absorption by
512 aerosols is affected by organic carbon. *Journal of Geophysical Research: Atmospheres*. 109.
513 <https://doi.org/10.1029/2004JD004999>, 2004.

514 Laskin, A., Laskin, J., Nizkorodov, S. A.: Chemistry of Atmospheric Brown Carbon. *Chemical Reviews*. 115,
515 4335-4382. <https://doi.org/10.1021/cr5006167>, 2015.

516 Li, Y., Fu, T.-M., Yu, J. Z., Zhang, A., Yu, X., Ye, J., Zhu, L., Shen, H., Wang, C., Yang, X., Tao, S., Chen, Q., Li,
517 Y., Li, L., Che, H., Heald, C. L.: Nitrogen dominates global atmospheric organic aerosol absorption. *Science*. 387,
518 989-995. <https://doi.org/10.1126/science.adr4473>, 2025.

519 Lin, P., Huang, X.-F., He, L.-Y., Zhen Yu, J.: Abundance and size distribution of HULIS in ambient aerosols at a
520 rural site in South China. *Journal of Aerosol Science*. 41, 74-87. <https://doi.org/10.1016/j.jaerosci.2009.09.001>, 2010.

521 Lin, P., Bluvshstein, N., Rudich, Y., Nizkorodov, S. A., Laskin, J., Laskin, A.: Molecular Chemistry of
522 Atmospheric Brown Carbon Inferred from a Nationwide Biomass Burning Event. *Environmental Science &*
523 *Technology*. 51, 11561-11570. <https://doi.org/10.1021/acs.est.7b02276>, 2017.

524 Liu-Kang, C., Gallimore, P. J., Liu, T., Abbatt, J. P. D.: Photoreaction of biomass burning brown carbon aerosol
525 particles. *Environmental Science: Atmospheres*. 2, 270-278. <https://doi.org/10.1039/d1ea00088h>, 2022.

526 Liu, D., He, C., Schwarz, J. P., Wang, X.: Lifecycle of light-absorbing carbonaceous aerosols in the atmosphere.
527 npj Climate and Atmospheric Science. 3, 40. <https://doi.org/10.1038/s41612-020-00145-8>, 2020.

528 Liu, Y., Huang, R.-J., Lin, C., Yuan, W., Li, Y. J., Zhong, H., Yang, L., Wang, T., Huang, W., Xu, W., Huang, D.
529 D., Huang, C.: Nitrate-Photolysis Shortens the Lifetimes of Brown Carbon Tracers from Biomass Burning.
530 Environmental Science & Technology. 59, 640-649. <https://doi.org/10.1021/acs.est.4c06123>, 2025.

531 Magalhães, A. C. O., Esteves da Silva, J. C. G., Pinto da Silva, L.: Density Functional Theory Calculation of the
532 Absorption Properties of Brown Carbon Chromophores Generated by Catechol Heterogeneous Ozonolysis. ACS Earth
533 and Space Chemistry. 1, 353-360. <https://doi.org/10.1021/acsearthspacechem.7b00061>, 2017.

534 Müller, S., Giorio, C., Borduas-Dedekind, N.: Tracking the Photomineralization Mechanism in Irradiated Lab-
535 Generated and Field-Collected Brown Carbon Samples and Its Effect on Cloud Condensation Nuclei Abilities. ACS
536 Environmental Au. 3, 164-178. <https://doi.org/10.1021/acsenvironau.2c00055>, 2023.

537 Qiu, Y., Qiu, T., Wu, Z., Liu, Y., Fang, W., Man, R., Liu, Y., Wang, J., Meng, X., Chen, J., Liang, D., Guo, S., Hu,
538 M.: Observational Evidence of Brown Carbon Photobleaching in Urban Atmosphere at Molecular Level.
539 Environmental Science and Technology Letters. 11, 1032-1039. <https://doi.org/10.1021/acs.estlett.4c00647>, 2024.

540 Saleh, R., Marks, M., Heo, J., Adams, P. J., Donahue, N. M., Robinson, A. L.: Contribution of brown carbon and
541 lensing to the direct radiative effect of carbonaceous aerosols from biomass and biofuel burning emissions. Journal of
542 Geophysical Research: Atmospheres. 120, 2102-2110, 2015. <https://doi.org/10.1002/2015JD023697>, 2015.

543 Saleh, R.: From Measurements to Models: Toward Accurate Representation of Brown Carbon in Climate
544 Calculations. Current Pollution Reports. 6, 90-104. <https://doi.org/10.1007/s40726-020-00139-3>, 2020.

545 Schnitzler, E. G., Abbatt, J. P. D.: Heterogeneous OH oxidation of secondary brown carbon aerosol. Atmospheric
546 Chemistry and Physics. 18, 14539-14553. <https://doi.org/10.5194/acp-18-14539-2018>, 2018.

547 Schnitzler, E. G., Gerrebos, N. G. A., Carter, T. S., Huang, Y., Heald, C. L., Bertram, A. K., Abbatt, J. P. D.: Rate
548 of atmospheric brown carbon whitening governed by environmental conditions. Proceedings of the National Academy
549 of Sciences. 119, e2205610119. <https://doi.org/10.1073/pnas.2205610119>, 2022.

550 Shan, M., Carter, E., Baumgartner, J., Deng, M., Clark, S., Schauer, J. J., Ezzati, M., Li, J., Fu, Y., Yang, X.: A
551 user-centered, iterative engineering approach for advanced biomass cookstove design and development. Environ. Res.
552 Lett. 12, 095009. [10.1088/1748-9326/aa804f](https://doi.org/10.1088/1748-9326/aa804f), 2017.

553 Shen, Y., Pokhrel, R. P., Sullivan, A. P., Levin, E. J. T., Garofalo, L. A., Farmer, D. K., Permar, W., Hu, L., Toohey,
554 D. W., Campos, T., Fischer, E. V., Murphy, S. M.: Understanding the mechanism and importance of brown carbon
555 bleaching across the visible spectrum in biomass burning plumes from the WE-CAN campaign. Atmospheric
556 Chemistry and Physics. 24, 12881-12901. <https://doi.org/10.5194/acp-24-12881-2024>, 2024.

557 Wang, Q., Zhou, Y., Ma, N., Zhu, Y., Zhao, X., Zhu, S., Tao, J., Hong, J., Wu, W., Cheng, Y., Su, H.: Review of
558 Brown Carbon Aerosols in China: Pollution Level, Optical Properties, and Emissions. Journal of Geophysical
559 Research: Atmospheres. 127, e2021JD035473. <https://doi.org/10.1029/2021JD035473>, 2022.

560 Wang, X., Heald, C. L., Ridley, D. A., Schwarz, J. P., Spackman, J. R., Perring, A. E., Coe, H., Liu, D., Clarke,

561 A. D.: Exploiting simultaneous observational constraints on mass and absorption to estimate the global direct radiative
562 forcing of black carbon and brown carbon. *Atmospheric Chemistry and Physics*. 14, 10989-11010.
563 <https://doi.org/10.5194/acp-14-10989-2014>, 2014.

564 Wang, X., Heald, C. L., Liu, J., Weber, R. J., Campuzano-Jost, P., Jimenez, J. L., Schwarz, J. P., Perring, A. E.:
565 Exploring the observational constraints on the simulation of brown carbon. *Atmospheric Chemistry and Physics*. 18,
566 635-653. <https://doi.org/10.5194/acp-18-635-2018>, 2018.

567 Wang, X., Chakrabarty, R. K., Schwarz, J. P., Murphy, S. M., Levin, E. J. T., Howell, S. G., Guo, H., Campuzano-
568 Jost, P., Jimenez, J. L.: Dark brown carbon from biomass burning contributes to significant global-scale positive
569 forcing. *One Earth*. 8, 101205. <https://doi.org/10.1016/j.oneear.2025.101205>, 2025.

570 Wang, Y., Hu, M., Lin, P., Guo, Q., Wu, Z., Li, M., Zeng, L., Song, Y., Zeng, L., Wu, Y., Guo, S., Huang, X., He,
571 L.: Molecular Characterization of Nitrogen-Containing Organic Compounds in Humic-like Substances Emitted from
572 Straw Residue Burning. *Environmental Science & Technology*. 51, 5951-5961.
573 <https://doi.org/10.1021/acs.est.7b00248>, 2017.

574 Wang, Y., Hu, M., Lin, P., Tan, T., Li, M., Xu, N., Zheng, J., Du, Z., Qin, Y., Wu, Y., Lu, S., Song, Y., Wu, Z.,
575 Guo, S., Zeng, L., Huang, X., He, L.: Enhancement in Particulate Organic Nitrogen and Light Absorption of Humic-
576 Like Substances over Tibetan Plateau Due to Long-Range Transported Biomass Burning Emissions. *Environmental*
577 *Science & Technology*. 53, 14222-14232. <https://doi.org/10.1021/acs.est.9b06152>, 2019.

578 Wong, J. P. S., Tsagkaraki, M., Tsiodra, I., Mihalopoulos, N., Violaki, K., Kanakidou, M., Sciare, J., Nenes, A.,
579 Weber, R. J.: Atmospheric evolution of molecular-weight-separated brown carbon from biomass burning. *Atmospheric*
580 *Chemistry and Physics*. 19, 7319-7334. <https://doi.org/10.5194/acp-19-7319-2019>, 2019.

581 Xiong, R., Li, J., Zhang, Y., Zhang, L., Jiang, K., Zheng, H., Kong, S., Shen, H., Cheng, H., Shen, G., Tao, S.:
582 Global brown carbon emissions from combustion sources. *Environmental Science and Ecotechnology*. 12, 100201.
583 <https://doi.org/10.1016/j.ese.2022.100201>, 2022.

584 Xu, L., Lin, G., Liu, X., Wu, C., Wu, Y., Lou, S.: Constraining Light Absorption of Brown Carbon in China and
585 Implications for Aerosol Direct Radiative Effect. *Geophysical Research Letters*. 51, e2024GL109861.
586 <https://doi.org/10.1029/2024GL109861>, 2024.

587 Yang, L., Huang, R.-J., Yuan, W., Huang, D. D., Huang, C.: pH-Dependent Aqueous-Phase Brown Carbon
588 Formation: Rate Constants and Implications for Solar Absorption and Atmospheric Photochemistry. *Environmental*
589 *Science & Technology*, 1236-1243. <https://doi.org/10.1021/acs.est.3c07631>, 2024.

590 Yue, S., Zhu, J., Chen, S., Xie, Q., Li, W., Li, L., Ren, H., Su, S., Li, P., Ma, H., Fan, Y., Cheng, B., Wu, L., Deng,
591 J., Hu, W., Ren, L., Wei, L., Zhao, W., Tian, Y., Pan, X., Sun, Y., Wang, Z., Wu, F., Liu, C.-Q., Su, H., Penner, J. E.,
592 Pöschl, U., Andreae, M. O., Cheng, Y., Fu, P.: Brown carbon from biomass burning imposes strong circum-Arctic
593 warming. *One Earth*. 5, 293-304. <https://doi.org/10.1016/j.oneear.2022.02.006>, 2022.

594 Yue, X., Mickley, L. J., Logan, J. A., Kaplan, J. O.: Ensemble projections of wildfire activity and carbonaceous
595 aerosol concentrations over the western United States in the mid-21st century. *Atmospheric Environment*. 77, 767-
596 780. <https://doi.org/10.1016/j.atmosenv.2013.06.003>, 2013.

597 Zeng, L., Zhang, A., Wang, Y., Wagner, N. L., Katich, J. M., Schwarz, J. P., Schill, G. P., Brock, C., Froyd, K. D.,
598 Murphy, D. M., Williamson, C. J., Kupc, A., Scheuer, E., Dibb, J., Weber, R. J.: Global Measurements of Brown
599 Carbon and Estimated Direct Radiative Effects. *Geophysical Research Letters*. 47, e2020GL088747.
600 <https://doi.org/10.1029/2020GL088747>, 2020.

601 Zeng, Y., Ning, Y., Shen, Z., Zhang, L., Zhang, T., Lei, Y., Zhang, Q., Li, G., Xu, H., Ho, S. S. H., Cao, J.: The
602 Roles of N, S, and O in Molecular Absorption Features of Brown Carbon in PM_{2.5} in a Typical Semi-Arid Megacity
603 in Northwestern China. *Journal of Geophysical Research: Atmospheres*. 126, e2021JD034791.
604 <https://doi.org/10.1029/2021JD034791>, 2021.

605 Zhang, Q., Wang, Y., Xiao, Q., Geng, G., Davis, S. J., Liu, X., Yang, J., Liu, J., Huang, W., He, C., Luo, B.,
606 Martin, R. V., Brauer, M., Randerson, J. T., He, K.: Long-range PM_{2.5} pollution and health impacts from the 2023
607 Canadian wildfires. *Nature*. <https://doi.org/10.1038/s41586-025-09482-1>, 2025.

608 Zhang, X., Chen, S., Kang, L., Yuan, T., Luo, Y., Alam, K., Li, J., He, Y., Bi, H., Zhao, D.: Direct Radiative
609 Forcing Induced by Light-Absorbing Aerosols in Different Climate Regions Over East Asia. *Journal of Geophysical
610 Research: Atmospheres*. 125, e2019JD032228. <https://doi.org/10.1029/2019JD032228>, 2020.

611 Zhao, R., Mungall, E. L., Lee, A. K. Y., Aljawhary, D., Abbatt, J. P. D.: Aqueous-phase photooxidation of
612 levoglucosan – a mechanistic study using aerosol time-of-flight chemical ionization mass spectrometry
613 (Aerosol ToF-CIMS). *Atmospheric Chemistry and Physics*. 14, 9695-9706. <https://doi.org/10.5194/acp-14-9695-2014>,
614 2014.

615 Zhao, R., Lee, A. K. Y., Huang, L., Li, X., Yang, F., Abbatt, J. P. D.: Photochemical processing of aqueous
616 atmospheric brown carbon. *Atmospheric Chemistry and Physics*. 15, 6087-6100. [https://doi.org/10.5194/acp-15-6087-](https://doi.org/10.5194/acp-15-6087-2015)
617 [2015](https://doi.org/10.5194/acp-15-6087-2015), 2015.

618